

STRUCTURAL DESIGN OF THE FLEXIBLY FORMED, MESH-REINFORCED CONCRETE SANDWICH SHELL ROOF OF NEST HILO

Diederik VEENENDAAL¹, Jack BAKKER² and Philippe BLOCK³

ETH Zurich, Institute of Technology in Architecture, Block Research Group
Stefano-Franscini-Platz 1, HIB E 45, 8093 Zurich, Switzerland
¹veenendaal@arch.ethz.ch, ³block@arch.ethz.ch

ZJA Zwarts & Jansma Architects
Pedro de Medina 1-9, 1086 XK, Amsterdam-IJburg, Netherlands
²jtb@zwarts.jansma.nl

Editor's Note: Manuscript submitted 20 September 2016; revision received 8 February 2017; accepted 8 March. This paper is open for written discussion, which should be submitted to the IASS Secretariat no later than September 2017. This paper is adapted from a publication in the proceedings of the 2015 IASS Symposium and published here with permission of the editors of the proceedings of the IASS 2015: International Symposium on Shell and Spatial Structures, held in August 2015, Amsterdam, Netherlands.

DOI: <https://doi.org/10.20898/j.iass.2017.191.847>

ABSTRACT

This paper describes the geometry and structural design of a flexibly formed, mesh-reinforced sandwich shell roof, as part of the NEST HiLo project, to be built in Dübendorf, Switzerland, in 2016. The computational design process consists of an integrated parametric model used for multi-objective evolutionary shape optimization of the shell, and subsequent analysis of its nonlinear behaviour.

Keywords: form finding, optimization, shell, flexible formwork, sandwich structure, ferrocement, TRC

1. INTRODUCTION

Thin-shell concrete structures are structurally efficient systems for covering large areas. However, their construction has seen a sharp decline since their golden era, between the 1920s and early 1960s, with the possible exception of air-inflated domes. Commonly cited reasons for their disappearance are the cost of formwork, and the rising cost of associated labour, and the declining interest from architects, possibly related to the limitations of geometries suitable to shell structures [17]. A revived interest in shell structures can be attributed to their formal similarity to doubly curved form in contemporary architecture.

This paper details the structural design and optimization for a new concrete shell roof that addresses these issues. The project aims to reduce construction cost and increase attractiveness of shell design and is designed such that it can be constructed with a reusable and lightweight flexible formwork system [29]. A flexible formwork allows the construction of a wide range of anticlastic shapes. The resulting shape can be even more

efficient than traditional analytical forms such as the hyperbolic paraboloid.

2. CONTEXT

This paper describes the geometry and structural design of the HiLo roof at the final design stage prior to detailed engineering and tendering i.e. the 'Bauprojekt' stage in Swiss code SIA 102. HiLo is a research & innovation unit within the NEST building [19] demonstrating ultra-lightweight construction and active building systems (Figure 1).

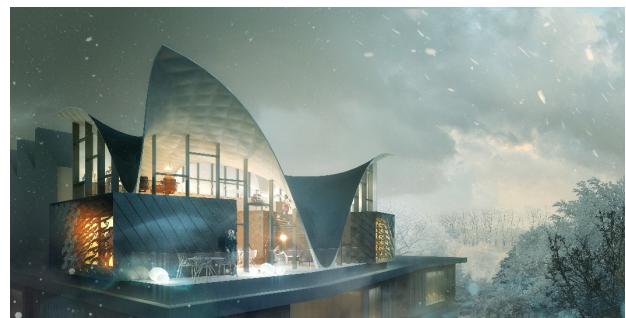


Figure 1: Visualisation of final design stage of HiLo (render by Doug&Wolf)

HiLo is planned as a 16m×9m duplex penthouse apartment for visiting faculty of Swiss federal research institutes Empa and Eawag to be completed in 2016 in Dübendorf, Switzerland. The project is a collaborative effort of the Block Research Group (BRG) and the Architecture and Building Systems Group (A/S), both at the Institute of Technology in Architecture, ETH Zurich, joined by architectural offices Supermanoeuvre and ZJA Zwarts & Jansma Architects. Structural engineers for the project are Bollinger + Grohmann Ingenieure. HiLo introduces several innovations, and this paper focuses on the development of the roof.

3. STRUCTURAL DESCRIPTION

The roof of HiLo is an anticlastic, thin shell structure to be constructed using a prestressed, cable-net and fabric formwork. The shell has a concrete thickness varying between 3 and 30cm, 8cm on average, features spans in the range of 6-9m and is supported on five 'touch-down' points with free edges along its entire perimeter. The shell is built up as a sandwich composite consisting of ferrocement or textile-reinforced concrete faces, and a rigid polyurethane (PU) core.

3.1. Anticlastic shell structures

Typical anticlastic shells are hyperbolic paraboloids, or hypars, which include some of the thinnest known shell structures, particularly those of Félix Candela. These shapes are ruled surfaces, exploiting the use of straight timber in their formworks. Slight improvements to their geometry can drastically improve their structural behaviour [25]. Such deviations can be achieved for example by using a prestressed cable-net and fabric formwork system allowing the roof of HiLo to depart from the traditional hypar.

3.2. Imperfection insensitivity

Hypars and negative curvature geometries in general are less sensitive to imperfection, and becomes insensitive with sufficient curvature [2,9]. This suggests that the post buckling behaviour of the shell does not govern i.e. the load factor does not decrease with increasing deflection, and this seems true for HiLo's roof. In accordance with IASS1979 recommendations, a factor of safety of 1.75 can then be taken. In addition, a series of

closely spaced eigenvalues is typically seen as an indication that a structure is imperfection sensitive, and indeed the opposite is observed in our case.

3.3. Creep and shrinkage sensitivity

On the other hand, gabled roofs with shallow hyperbolic parabolas are particularly sensitive to time-dependent deformation, and there have been specific instances of such structural failures [6]. Including creep and shrinkage can lead to 25-50% reduction in load carrying capacity and a four- to eightfold increase in displacements. Shallowness is defined by two criteria:

- $\text{rise} / \text{span} < 0.2$
- $\text{rise} \cdot \text{thickness} / (\text{first span} \cdot \text{second span}) > 0.003$ (for saddle roofs)

Although HiLo's roof does not meet these criteria, a substantial reduction in load carrying capacity due to creep and shrinkage has been observed in our case as well. This long-term behaviour is dependent on the concrete strength (as a function of the water/cement ratio). The influence of strength class on the load factor was evaluated by varying between C35 and C90. Results inform further detailed analysis and concrete mix development.

3.4. Thin, free edges

Unlike historical hypars with straight edges, HiLo's roof shell has no edge beams, but features thin edges, thickening towards the five supports. The shell is not supported by the facade mullions, which only transmit horizontal wind loads to the shell. The shell has no internal ribs, unlike traditional shells composed of multiple hypars. For single or gabled hypar roofs, reducing or entirely removing any edge beam (possibly thickening the shell at the supports) decreases overall shell bending [10,20]. Although maximum displacements may increase, they are not significant compared to serviceability limits.

Kollár and Dulácska [12] claim, based on a synclastic model test, that shells with free edges exhibit global rather than local buckling, and may have increasing load capacity after buckling, provided that internal forces can shift to the interior and this inner part is able to carry more load than the original load paths in compression. Tomás and Tovar [26] show results for hypars which become imperfection insensitive if only the corners instead of the edges are supported.

3.5. Sandwich section

The shell is subject to strict requirements for energy performance. The required U-value is 0.17 W/m K and the overall apartment is supposed to generate a 40-50% annual weighted energy surplus. The roof is used as a solar collector for electrical and possibly thermal energy on the outside, and as a low energy radiant heating and cooling system on the inside, requiring the inside concrete surface to remain exposed.

To minimise thermal bridging, the connection between the glass facade and shell led to the present sandwich design (Figure 2). Although intuitively the sandwich would seem to present only structural benefits by increasing structural depth and reducing sensitivity to external loads and imperfections, the differences in temperature and humidity on either side of the PU core lead to higher thermal loads and differential strains due to creep and shrinkage.

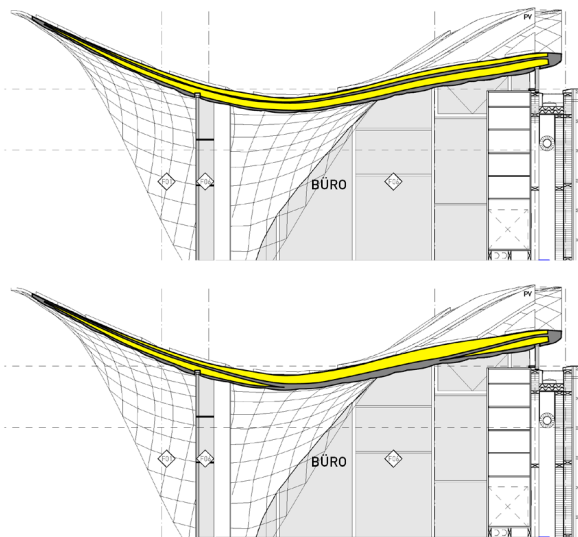


Figure 2: Roof section of HiLo with full sandwich, and alternative with sandwich locally along glass facade (adapted from drawing by Supermanoeuvre)

For this reason, but also to reduce complexity during construction, an alternative has been calculated in which the sandwich only occurs along the glass and the interior part of the shell is a single layer.

3.6. Mesh reinforcement

Due to the thinness of the shell and various unfavourable load cases and combinations, the shell will locally act in bending and thus needs to be

reinforced accordingly. The shell can be reinforced using woven (or welded) meshes made of (Figure 3):

- steel where the composite is called "ferrocement"; and
- alkaline resistant (AR) glass-fibre; or,
- carbon-fibre where the composite is called "textile reinforced concrete" (TRC).

Ferrocement will allow us to maintain thinness, by following curvatures more easily than traditional rebar, and requiring only minimal cover of 2mm (ACI 549R-97). Compared to conventional reinforced concrete, ferrocement has a fine mortar matrix with densely distributed reinforcement leading to high ductility with homogenous, isotropic properties (including high tensile strength), as well as high durability due to very small crack widths and spacing [18]. Textile-reinforced concrete (TRC) with glass or carbon fibre offer similar benefits, but is even more flexible.

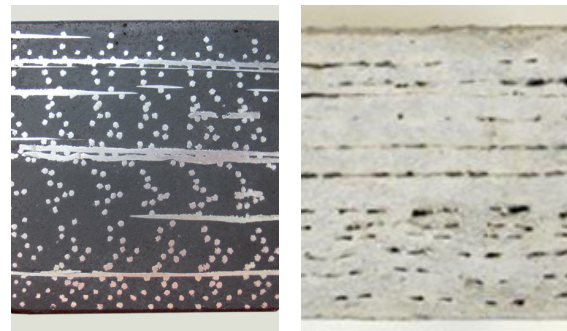


Figure 3: Examples of ferrocement and carbon-fibre TRC sections, 50mm thick, showing dense mesh reinforcement [3,24]

The decision for the final material of the reinforcement mesh (steel, carbon or AR glass) will be made in the next phase. Due to its high in-plane thermal conductivity, ferrocement is currently favoured as reinforcement for the thermally active roof. Potentially the materials can be combined to improve thermal conductivity only for the interior part of the shell, while suppressing it at the connection to the glass facade and at the exterior. A combination with fewer mesh layers with fiber reinforcement is also being considered.

3.7. Prestressed flexible formwork

The shell is anticlastic everywhere, as it will be constructed on a prestressed grid with fabric shuttering, which is lightweight and easily

transported. Without the need for scaffolding directly underneath, there is no need for temporary foundations and unobstructed access is made possible.

Three structures are known to have been built with a cable-net formwork, using materials other than fabric as shuttering. A London City Council school assembly hall consisting of five 22m span, 100mm thin hypars, in Southwark, Newington, London, UK, now the Pentagon Hall at the Ark Global Academy, was built around 1960 following a 1:8 prototype (Figure 4) [4,5]. In this case, some of the wires were left for post-tensioning. The shuttering was mesh reinforcement and woodwool insulation, and c. C50/60 shotcrete ('Gunite') was applied directly from underneath. This underlines the benefit of unobstructed access when using flexible formworks.



Figure 4: Pentagon Hall, London, UK, built c. 1960, and Auto Perfection car repair shop, Midland, MI, USA, built c. 1960-1962 (above: © Mike Deakin, below: CC BY 4.0 Ryan Collier)

Around the same time, c. 1960-1962, but independently, the Bay Service Station in Midland, MI, USA [13], now the Auto Perfection car repair shop (Figure 4), and a clubhouse at the Purdue Golf Course in West Lafayette, IN, USA [32], demolished in the mid-1990s, were built, both an assembly of four 14m span, 165mm thin hypars. Earlier prototypes, up to 5:8 in scale, are described in [31]. In this case, the shuttering was XPS foam

insulation, while the cable-net was lost formwork for traditionally placed c. C45/55 concrete.

In these cases, substantial deviations from the design shape due to deflections are reported. Van Mele and Block [27] presented a method for finding the distribution of forces to obtain a particular shape, after it has been loaded with fresh concrete. This control allows a range of pre-defined, non-analytical, anticlastic shapes to be designed and constructed, with much greater accuracy [29,30].

4. FORM FINDING AND OPTIMIZATION PROCESS

The design process for the roof consists of an integrated parametric model used for multi-objective evolutionary optimization of the shell, and subsequent analysis of its nonlinear behaviour as well as the flexible formwork used for its construction. Figure 5 explains the computational design process of HiLo, consisting of form generation, structural analysis, and multi-criteria shape optimization.

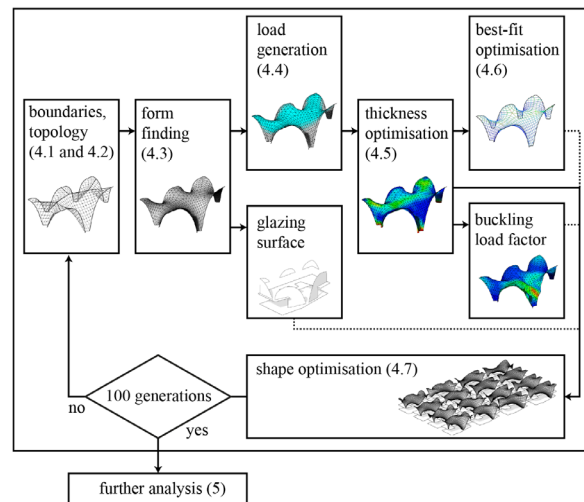


Figure 5: Workflow of optimization and analysis (sections in parentheses), additional criteria in dotted lines

The process consists of boundary, topology and form generation (Sections 4.1, 4.2, 4.3). Then load generation (Section 4.4) to allow for thickness optimization (Section 4.5). The shell geometry and mass is now fixed and can be evaluated for further for cable-net forces (Section 4.6) as well as the amount of glazing along its perimeter. These parameters were then used to inform the shape optimization (Section 4.7). Some details on the implementation are provided in Section 4.8, before

continuing with the further analysis after optimization (Section 5).

The geometry that is initially generated is maintained throughout the entire process, acting both as the layout of the cable net and the mesh of the shell itself (apart from triangulation, some nodes inserted to apply wind loads from the glass façade, and subdivision for further analysis in Section 5).

4.1. Boundary generation

The shape of the roof is largely determined by the geometry of its boundary edges, and the topology of the generating network. The edge consists of four or five undulations, one for each support, curving between each support position to the given height h of the roof. Each half undulation is characterised by an amplitude $a = h$, period p , and sharpness s (Figure 6):

$$z(t) = a \cos^2\left(t(x) \frac{\pi}{2p}\right) \quad (1)$$

$$\text{where } t(x) = \frac{s \cdot x + x}{s \cdot x + 1}.$$

In a first optimization, four or five support positions, determining p , the sharpnesses s , and the roof height h were parameters for the optimization, i.e. seven or eleven variables for optimization.

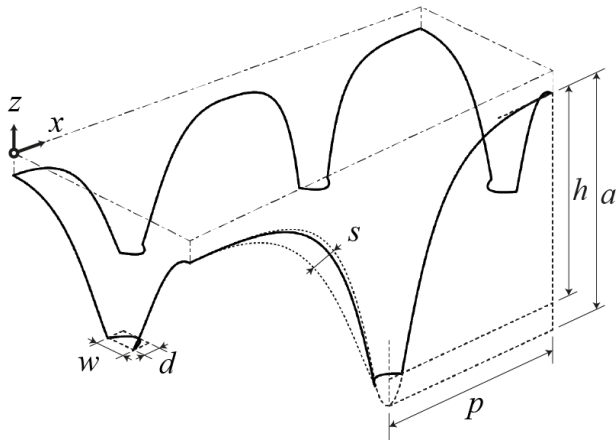


Figure 6: Boundary generation

The boundary curves can extend below the foundation and can optionally be cut off. By doing this, the roof touches down on the floor with a planar, curved footprint. These are defined as parabolas with a certain width w and depth d ; two

additional parameters for the edge shape (Figure 6). The resulting space is required for the exterior insulation, drainage, connections to the thin-film photovoltaics and hydronic system, providing effective area for the supports, and ensuring that the glass façade connects to the shell at angles of $\pm 45^\circ$ to allow for proper detailing.

In this case, the sharpness s can be determined from a height h , period p , width w and amplitude a :

$$s = -\frac{c + \pi n}{n(c + 2\pi n - \pi)} \quad (2)$$

$$\text{where } c = \arccos(2h/a - 1) \text{ and } n = \frac{1}{2} \frac{w}{p}.$$

In the final optimization, the five support positions were fixed, leaving three parameters for optimization: width w , amplitude a , depth d , i.e. fifteen variables for optimization.

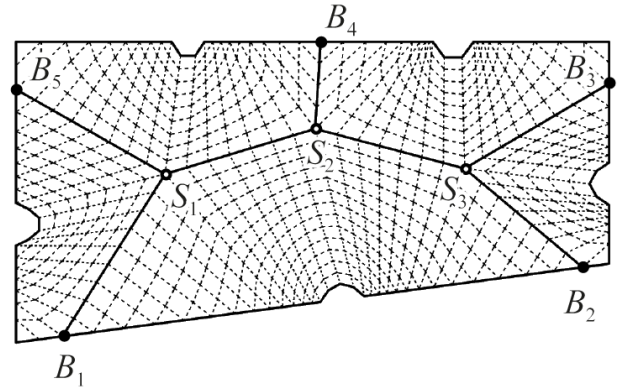


Figure 7: Topology generation

4.2. Topology generation

The roof is then divided into five convex patches, determined by five points B_i on the shell's boundary and three interior points S_i (Figure 7), which are subdivided as follows (Figure 8).

Each patch is then subdivided along approximately radial and concentric directions with respect to the support positions.

The interior edges of the patch are divided into an equal number of segments that are as close as possible to some desired, global edge length. This same number then subdivides the exterior edges of the patch. The resulting vertices are connected to the corresponding vertices along the interior edges.

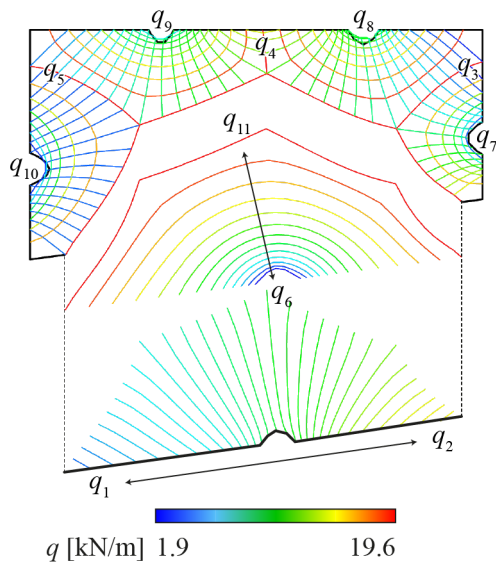


Figure 8: Force densities interpolated from eleven values

Starting at the outermost exterior vertices, concentric edges are created that follow the interior boundary of the patch, crossing all radial edges in between. For undulations that are cut off, the exterior vertices are divided evenly over the three exterior curve segments, based on their relative

lengths. The parabolic segments get at least three vertices, to avoid degrading them into straight lines.

4.3. Form generation

From these boundary conditions, a suitable, anticlastic shape is generated using the linear force density method [23]. To minimise the number of additional variables for optimization, the force densities throughout the network are determined by interpolating nine or eleven values for four or five supports respectively (Figure 5). The ratio of allowable force densities is limited to 1:20, to create reasonable shapes without too abrupt changes in curvature and resulting forces. In the case of cut-off supports, the network potentially curves in on itself (Figure 5). This is remedied by calculating force densities of the network's triangulated projection using the linear natural force density method [21]. This tends towards a minimal surface of our projection, avoiding overlaps, and thus any inward curving. These force densities are then used in a second form-finding procedure, which is also partially constrained to the original form-found mesh.

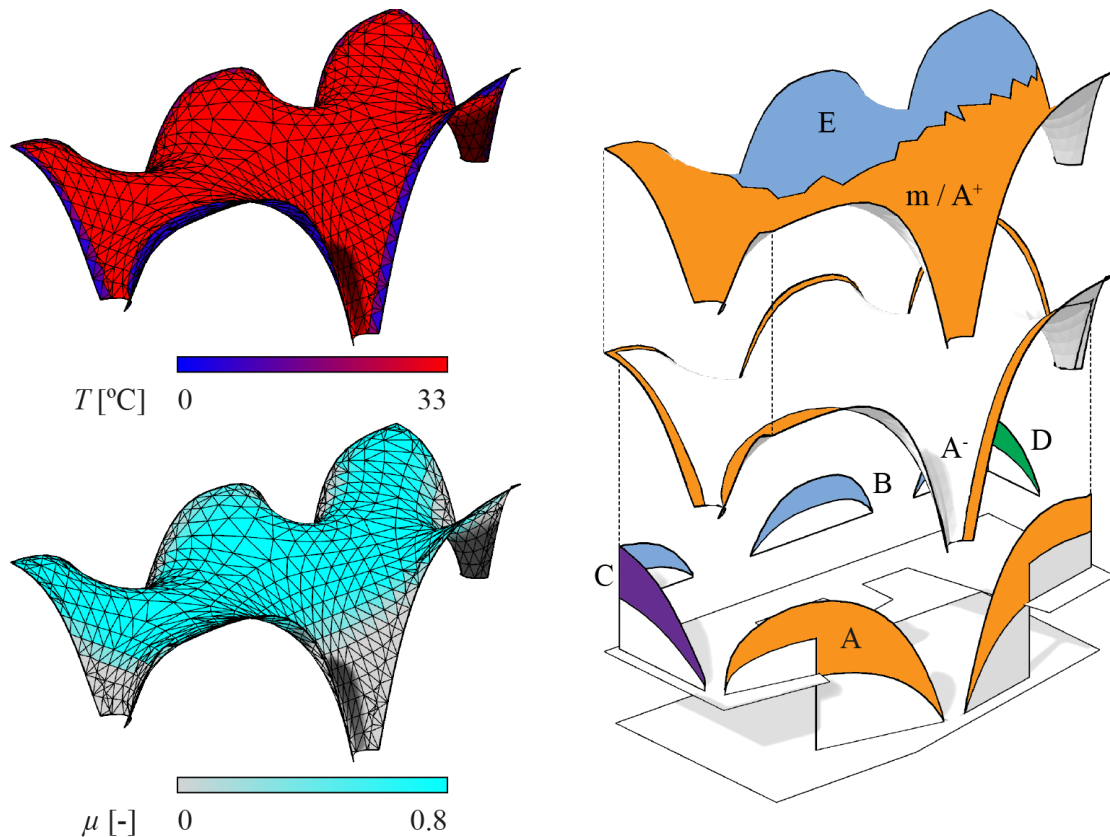


Figure 9: Load generation for thermal loads, snows loads and wind zones for main wind direction (SW) both for pressure (+) and suction (-)

Table 1: Reduction factors ψ , unfavourable/favourable load factors γ (SIA 260) and critical buckling load factor λ (IAASS 1979)

Load	Self-weight	Dead	Thermal	Live	Wind	Snow
SLS occasional $1.0 / \psi_0$	1.0	1.0 / 0.0	1.0 / 0.6	1.0 / 0.0	1.0 / 0.6	1.0 / 0.86
SLS frequent ψ_1 and ψ_2	1.0	1.0 / 0.0	0.5 / 0.0	0	0.5 / 0	0.43 / 0
SLS quasi-permanent ψ_2	1.0	0.7 (1.0)	1.0 (0.0)	0	0	0
ULS load factor γ	1.35 / 0.8	1.35 / 0.8	1.5 / 0	1.5 / 0	1.5 / 0	1.5 / 0
CLS load factor λ	1.75					

Table 2: Load combinations with and without thermal loads (LC) used. Leading action in bold

	Load	Self-weight	Dead	Thermal	Snow	Wind suction	Wind pressure	Live
SLS quasi-permanent	LC 0	1.0	0.7	0.2 / 0				
SLS occasional	LC 1	1.0	1.0	1.0 / 0	1.0			
	LC 2	1.0		1.0 / 0		1.0		
	LC 3	1.0		1.0 / 0			1.0	
	LC 4	1.0	1.0	1.0 / 0	0.86			1.0
ULS	LC 5	1.35	1.35	0.6 / 0	1.5			
	LC 6	0.80		0.6 / 0		1.5		
	LC 7	0.80		0.6 / 0			1.5	
	LC 8	1.35	1.35	0.6 / 0	0.86			1.5
	LC 9	1.35	1.35	1.5 / 0	0.86			

4.4. Load generation

For each shape, loads are automatically generated from SIA 261 to be applied to the structure. These loads include: the self-weight of the concrete (24 kN/m³); dead loads from the integrated shell (0.5 kN or 0.3 kN/m²); live loads for maintenance on the roof (1 kN or 0.4 kN/m²); thermal loads due to the embedded hydronic system for a minimum temperature of 0 °C for optimization (Figure 6) and -20 °C for final analysis; snow loads ($\mu \times 0.9$ kN/m², Figure 6); and wind loads ($C_p \times 1.07$ kN/m²). For the wind loads, half of the wind load on the glass facade is also taken into account. The snow shape factor μ varies between 0 and 0.8 depending on the roof angle and the wind shape factor varies between -0.3 and +0.75 depending on the wind direction and roof angle (we interpolate between facade and angled roof, i.e. zone A+ and m, in Figure 9).

Load combinations were defined using reduction factors ψ and load factors γ in Figure 7 following SIA 260. The quasi-permanent load combination is used for the determination of creep and shrinkage,

with dead loads and thermal loads altered (0.7 and 1.0 instead of 1.0 and 0.0) to reflect the actual long-term load on the shell. The occasional load combinations are used for checks in the serviceability limit state (SLS) against allowable deflections and crack width. They are also the starting point for limit load calculations. The ultimate limit state (ULS) load combinations are used to check against allowable stresses. Limit load calculations were carried out to establish whether the load factor λ , or safety factor, according to IAASS 1979 was met. This limit load state is here referred to as the ‘critical limit state’ (CLS).

4.5. Thickness optimization

By redistributing the material in the shell, it is possible to reduce the total volume of required concrete, even though the maximum stresses stay within the same limits. The program Karamba tries to approach a given maximum deflection of $L/500 = 18$ mm, while reducing thicknesses throughout the structure and keeping within a 20 MPa stress limit. The linear elastic stiffness was reduced to only $E = 5000$ MPa to approximately account for

cracking and creep in the design. The optimization is done for all SLS load combinations, as those in the ULS were found to not govern the results. The presented result has a minimum and average thickness of 3.0 and 7.7 cm, and a total weight of 29 metric tons.

4.6. Best-fit optimization

The goal is now to find the forces in the cable-net such that, under given loads of the wet concrete, the resulting concrete shell takes the form of the target shape [27]. The topology and shape of the cable net (Sections 4.2 and 4.3) is the basis for triangulated mesh of the shell (Section 4.4 and 4.5). To enforce reasonable bounds on these forces under load (4-50 kN along the perimeter), the resulting constrained linear least squares problem can be written as a quadratic program. Assuming the bounds have not allowed us to find an exact match with the target shape, we compute the sum of squared deviations, which are used as target for optimization. The constrained linear least squares solver offers an initial estimate of the force distribution, showing how different solutions compare, but within reasonable computational time. A more robust nonlinear algorithm [28] is applied to the final geometry to obtain the closest-fit in the detailed engineering and tendering phase, as the topology of the formwork may change depending on input from the future contractor.

4.7. Shape optimization

The roof was optimized in two rounds: initially, a single-criterion optimization; and then a final multi-criteria optimization. The optimization was carried out for a monolithic concrete shell, and the sandwich section was taken into account in the subsequent structural analysis (Section 5).

The first optimization minimized mass, proportional to the elastic bending energy E , subject to preliminary stress and deflection constraints (20 N/mm² and 30 mm). The energy is a function of the shape $f=f(x,s,h,q)$ with 16-22 variables (seven or eleven boundary parameters plus nine or eleven force density parameters, for shells with four or five supports respectively).

This stage studied different boundary conditions (positions and number of supports as well as roof

height), and their relative influence on the potential to minimize the mass. The problem is to:

$$\text{minimize } E(f(x,s,h,q))$$

subject to

$$\sigma \leq 20 \text{ N/mm}^2,$$

$$\delta \leq 30 \text{ mm},$$

$$0.11 \leq x_4 \leq 0.45,$$

$$0.60 \leq x_3 \leq 0.90,$$

$$1.10 \leq x_2 \leq 1.90,$$

$$2.10 \leq x_1 \leq 2.43,$$

$$3.45 \leq x_5 \leq 3.90,$$

$$0 \leq s_{1...5} \leq 10,$$

$$0 \leq h \leq 5, \text{ and}$$

$$1 \leq q_{1...11} \leq 10.$$

The bounds on variables x were determined to avoid any supports close to the corners, and keep any supports within the architecturally and functionally preferred support zones. The bounds on variable s were subjectively set to avoid extremely steep or shallow edge curves. The bounds on variable h were determined by a minimum ceiling clearance and a maximum allowable roof height.

The second and final multi-criteria optimization, subject to a preliminary stress and deflection constraints (20 N/mm² and 1/500th of the span L), minimized four criteria: internal elastic energy (proportional to mass) as before; the buckling load factor (lowest, positive value); deviations of the cable net to the target shape; and, surface area of glazing. A fifth measure of the amount of head clearance below the roof was also calculated to compare results, measured as the sum of squared lengths of all nodes higher than 2.15m. These criteria are all a function of the shape $f=f(w,d,a,q)$ with 26 variables (fifteen boundary and eleven force density parameters for a shell with five supports).

This stage determined the final design as it was submitted to the authorities for building permission (see also Sections 4.1-2). The problem is to:

minimize $E, -\lambda, \Delta \mathbf{z}^T \Delta \mathbf{z}, A$,
 as functions of $f(w, d, a, q)$,
 subject to

$$\begin{aligned} \sigma &\leq 20 \text{ N/mm}^2, \\ \delta &\leq L / 500, \\ 1.2 &\leq w_1 \leq 2.0, \\ 0.9 &\leq w_{2\dots 5} \leq 1.2, \\ 0.42 &\leq d_1 \leq 0.82, \\ 0.45 &\leq d_{2\dots 5} \leq 0.75, \\ 7.5 &\leq a_1 \leq 9.0, \\ 4.4 &\leq a_{2\dots 5} \leq 9.0, \\ 1 &\leq q_{1\dots 5, 11} \leq 20, \text{ and} \\ 1 &\leq q_{6\dots 10} \leq 10. \end{aligned}$$

The bounds on variables w , d and a , were set to maintain various requirements related to space for insulation and drainage on the exterior, and to angles between the shell and the glass façade on the interior.

4.8. Implementation

The entire design process was implemented in Grasshopper for Rhinoceros [14,22]. Several plugins for Grasshopper were included: Karamba for structural analysis, thickness optimization, Kangaroo for the second form-finding procedure

and Octopus for multi-objective optimization. Thermal actions were based on calculations carried out in Energy2D and ANSYS by A/S. A custom VB component generated the boundaries and topology, and custom IronPython components were written to communicate with external CPython scripts; the first form-finding procedure and calculation of prestresses in the cable-net formwork, the latter using CVXOPT's QP solver [1] to solve the bounded least-squares problem.

The shell was subsequently evaluated for various additional nonlinearities in Sofistik (see Section 5), as the present version of Karamba does not include layered or volume elements to model the sandwich, non-linear material models, or third order geometric nonlinearity to evaluate post-buckling behavior. However, Sofistik is also limited as it is not capable to combine volume elements with both non-linear material and geometric modelling, to load step thermal actions, and to model the reinforcement in more than two layers per side. The input for Sofistik is generated from Grasshopper using a custom IronPython component.

Karamba only offers 3-node triangular TRIC elements for shell analysis. The mesh was relatively coarse (Figure 10) to minimize computational time during optimization. Sofistik only offers 4-node, non-conforming, Mindlin-Reissner quadrilateral elements. The mesh was subdivided once to improve the accuracy, particularly the resolution of the buckling modes (Figure 11).

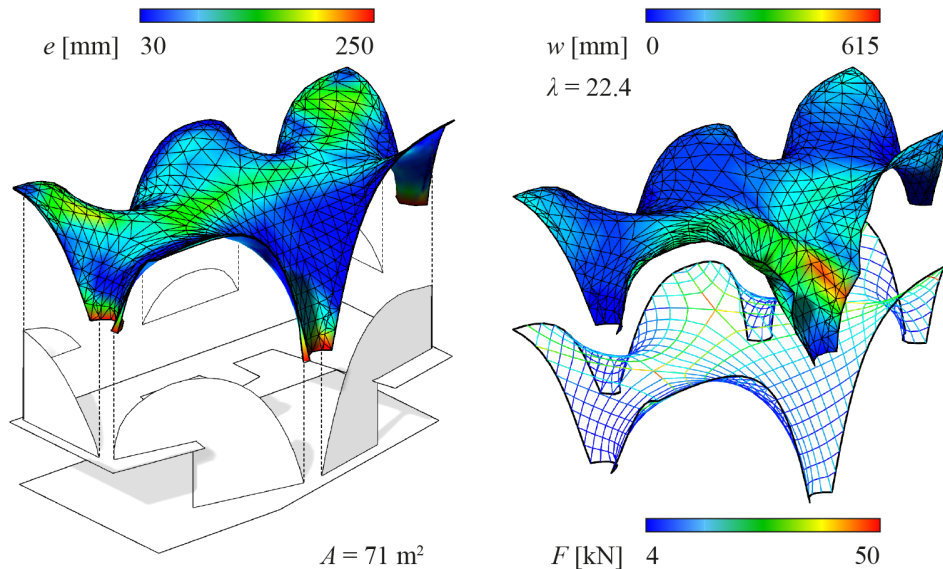


Figure 10: Four criteria: elastic energy (proportional to mass, shown as thickness e), buckling load factor λ for LC 0 (showing first positive buckling mode with deflection w), cable-net deviations (showing constrained forces F under load), and surface area A of clear glazing

5. STRUCTURAL ANALYSIS

The subsequent structural calculations, carried out in Sofistik, follow Swiss code SIA 262 - intended for conventional reinforced concrete - where possible, but applies ACI 549R-97 and ACI 549.1R-93 for aspects related to ferrocement, and Medwadowski et al. [16], here referred to as 'IASS 1979', for aspects related to thin-shell structural design. Creep and shrinkage formulas from SIA 262 are based on those in EN 1992-1-1:2004. Adopting IASS 1979 means that we are required to perform a stability analysis, by calculating the initial buckling load, or critical load, then modifying this load - or recalculating using a sufficiently refined model - by taking into account: large displacements (geometric nonlinearity), material properties of concrete and reinforcement (material nonlinearity including creep and shrinkage) and deviations from the idealised shape (imperfections). Because the research unit will be replaced after 5-10 years, the reference period for design is 20 years. Load combinations are according to Section 4.4.

5.1. Boundary conditions

As mentioned, the shell is supported on five locations. Those at the rear are close to the backbone, and assumed fixed. Those in front are supported on a cantilevering, prestressed concrete floor slab, which are modelled as springs (stiffnesses provided by structural engineers of the NEST building, Dr. Schwartz Consulting). One support is modelled as a horizontal spring as well to account for the local flexibility of the supporting steel frame.

5.2. Material properties

The reinforced concrete was modelled as a C90/105 with B500A according to SIA 262, but additional calculations were carried out for a range between C35 and C90 concrete, and for AR-glass and carbon fibre TRC, to inform the detailed engineering phase. The higher C90 concrete strength was mainly chosen based on the resulting creep and shrinkage behaviour according to code, and given previous experience with viscous and fine concrete mixes, which exhibit high strength [29]. The steel type was chosen based on its similarity to that mentioned in ACI 549.1R-93. The mesh layers are 1mm diameter, with 13mm spacing, so 60 mm²/m per direction, with up to 12 layers per concrete face. The PU is modelled based on linear elastic

properties from suppliers: $E = 300$ MPa, $f_y = 20$ MPa, $\rho = 600$ kg/m³.

The creep coefficients are $\phi = 1.06$ (inner face), 2.25 (PU foam insulation) and 0.81 (outer face). The drying shrinkage strains are $\epsilon = -0.19\%$ (inner face), -0.10% (outer face). Following SIA 262, autogeneous shrinkage is not included yet, pending development and testing of the actual concrete mix. The current values assume that the shell remains in the formwork while curing for 28 days, and that the average layer thickness is 50mm. The inner face is exposed on one side and has a relative humidity of 40%, while the outer face is completely enclosed and has a relative humidity of 60%. For the creep of the PU very little is known, and for now is taken from Garrido et al. [7], who investigated rigid PU foam for sandwich panels, though of much lower density.

The creep coefficients and shrinkage strains were applied to the quasi-permanent load combination in forty incremental steps, simulating 20 years of creep and shrinkage. This state was then used for further application of the occasional SLS and the ULS load combinations.

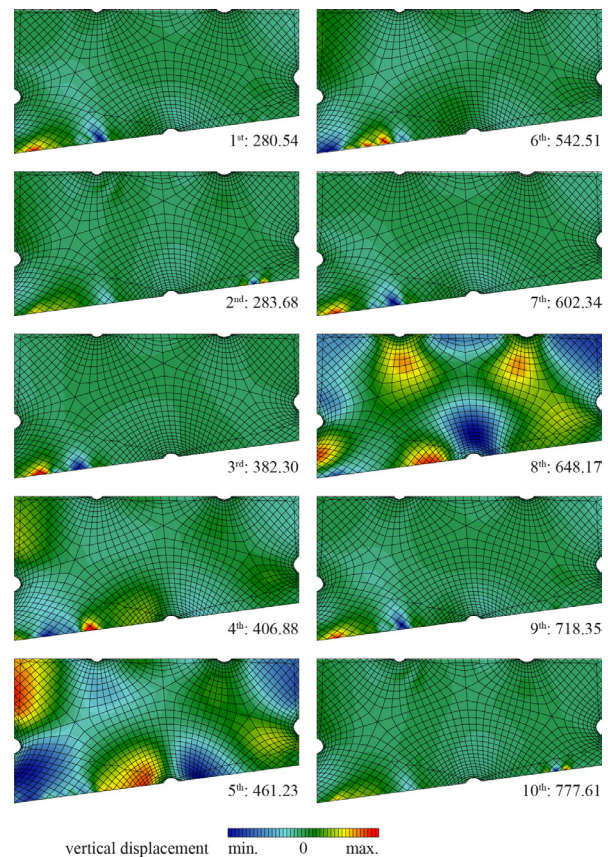


Figure 11: First ten positive buckling modes, with the fifth mode taken as the shape for the imperfection

5.3. Limit states

In SLS, allowable deflections for occasional live loads are 1/500th of the span L , i.e. 18mm for the shell, and 1/300th of twice a cantilever, i.e. 60mm for the cantilevering slab supporting the shell at the front (SIA 260). Deflections along the glass facade are chosen to be less than 10mm. Crack width may not exceed 0.1mm according to ACI 549R-97. In ULS, stresses should not exceed the material strengths and buckling with decreasing post-buckling capacity may not occur. In CLS, a limit load of more than 1.75 the SLS load combinations should be reached.

5.4. Imperfections

Tomas & Tovar [26] present an overview of how imperfections have been calculated for shell structures, and the most conservative combination of these formulas has been taken here.

It is assumed that the initial imperfection has the same shape as the first positive, globally acting buckling mode, with a magnitude of 39mm. The initial imperfection w_0 is simply the sum of the calculable imperfection w_0' and the accidental imperfection w_0'' (IASS 1979). The former is the maximum deflection obtained for a service load combination using linear elastic analysis. As an upper limit we can take the allowable deflection $w_0' = 18\text{mm}$ (Section 5.3). The latter is the accidental

imperfection due to erection inaccuracies, according to Medwadowski [15]:

$$w_0 = w_0' + w_0'' = 39\text{mm} \quad (3)$$

$$\text{where } w_0'' = 0.1e \left(1 + \frac{5a}{1 + \beta^{-2}} \right) = 21\text{mm}$$

$$\text{with } \beta = 0.001 \frac{\sqrt{R_1 R_2}}{e} = 0.13$$

in which $a = 6$ for a shell built using slipform (assumed to be similar to the flexible formwork; $a = 1$ for rigid formworks), e is the shell thickness, and R_1 and R_2 are the principal radii of curvature of the shell. It is assumed that the (area weighted) mean values can be taken, meaning that the thickness of the sandwich $e = 140\text{mm}$, and principal radii R_1 and R_2 are 25m and 14m respectively.

6. RESULTS

Figure 12 shows the results from the initial broader optimization varying position, height and number of supports, identifying greatest potential for structural and energy performance. Resulting shapes were analysed for mechanical properties (displacements, buckling load factor), geometric properties (thickness, surface area, enclosed volume, glazing surface), and total annual radiation.

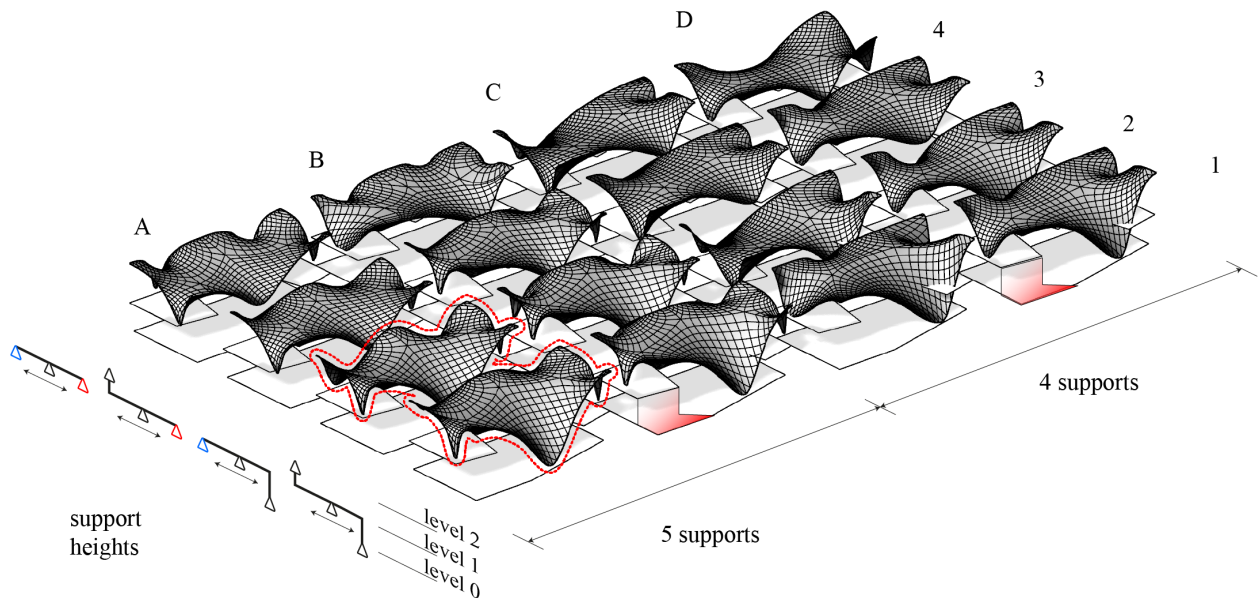


Figure 12: Results from sixteen early optimisations (16x 100 generations, 100 shells each), with A1 and A2 selected for further development based on

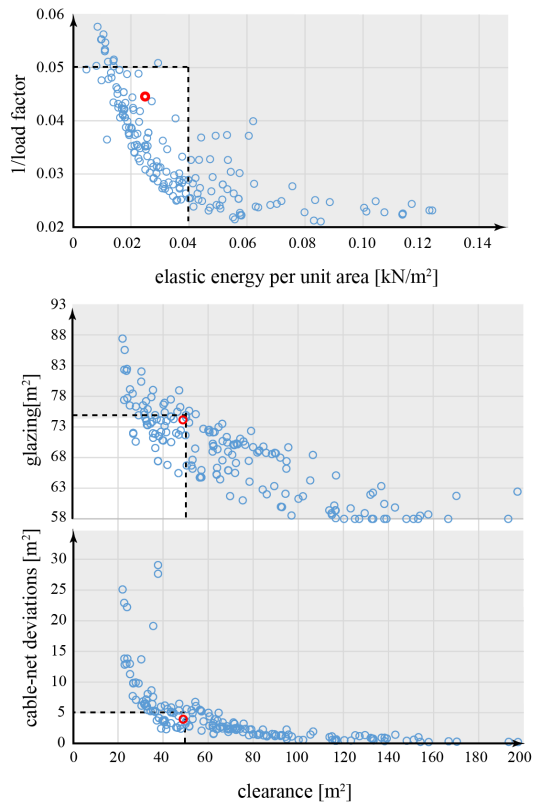


Figure 13: Projections of Pareto front from final multi-criteria optimization based on buckling load factor, elastic energy (proportional to mass), cable-net deviations, and glazing, showing a measure of head clearance below the roof as well. Limits on objective values shown as dotted lines. Final design shown in red

Based on initial optimization results, solutions A1 and A2 were chosen as the direction for further development. Main issues were the lack of head clearance at mezzanine level and vertical position of the supports in the back. The clearance was addressed by including it as a metric for evaluation, raising the roof level, and changing the mezzanine walkways to allow more space around the supports. The vertical position of the supports was set to be mezzanine level as in A2, to allow connection to the mezzanine and supporting building structure, and increase curvatures of the shell.

Figure 13 shows the results from the final multi-criteria optimization, weighing structural and energy performance against constructional considerations. The four criteria were internal elastic energy (proportional to mass), GNL buckling load factor (lowest, positive value), deviation of cable net to target shape, and surface area of glazing. A fifth measure of the amount of

head clearance below the roof was also calculated to compare results. The optimization was carried out for a monolithic concrete shell, and the sandwich section was taken into account in the subsequent structural analysis.

The structural capacity of the shell is limited by the steel stress in both SLS [≤ 410 MPa] and ULS [≤ 465 MPa], as well as the load factor in CLS [≥ 1.75].

Figure 14 plots the CLS load displacement diagrams for LC 1 and 4 with increasing nonlinearities, revealing the roughly bilinear behaviour of the shell, and the improving effect of thermal action on the load factor (Figure 14, blue versus red lines). While the linear load capacity is in the order of 1000, the lowest load factor is 3.0. As a final check on the post-buckling behaviour, Kollár [11] and Kollár & Dulácska [12] recommend to plot the displacement against the displacement over the load, a so-called Southwell plot. Figure 15 is a plot of LC 4 including thermal action and imperfection. The load P is taken to be equal to the total vertical reaction force. A straight line would indicate constant post-buckling behaviour; and upward curving line (as in our case) indicates increasing post-buckling behaviour (referred to as Case 1 by IASS 1979). The first part of our plot (up to 12 mm displacement) is unusual and is a result from Sofistik's inability to load step thermal actions (meaning the thermal action is always included with a load factor of 1, also distorting the rest of the plot).

The sandwich causes differential temperature and humidity, and thus differential creep and shrinkage strains, as well as thermal actions. The amount of creep and shrinkage seems to be the main determinant of the shell's capacity. The shell shows very small displacements, less than 10mm in SLS, and well below any limits. In fact, the stiffness of the shell is so substantial, that the concrete acts as in a restrained manner, with cold temperatures and subsequent contractions leading to micro-cracking throughout, rather than deformations. However, the inclusion of thermal action actually improves load factors, suggesting it acts as a form of prestress.

Further engineering of the roof will depend on development of the specific concrete mix, method of concrete placement, more detailed reinforcement layout and so on.

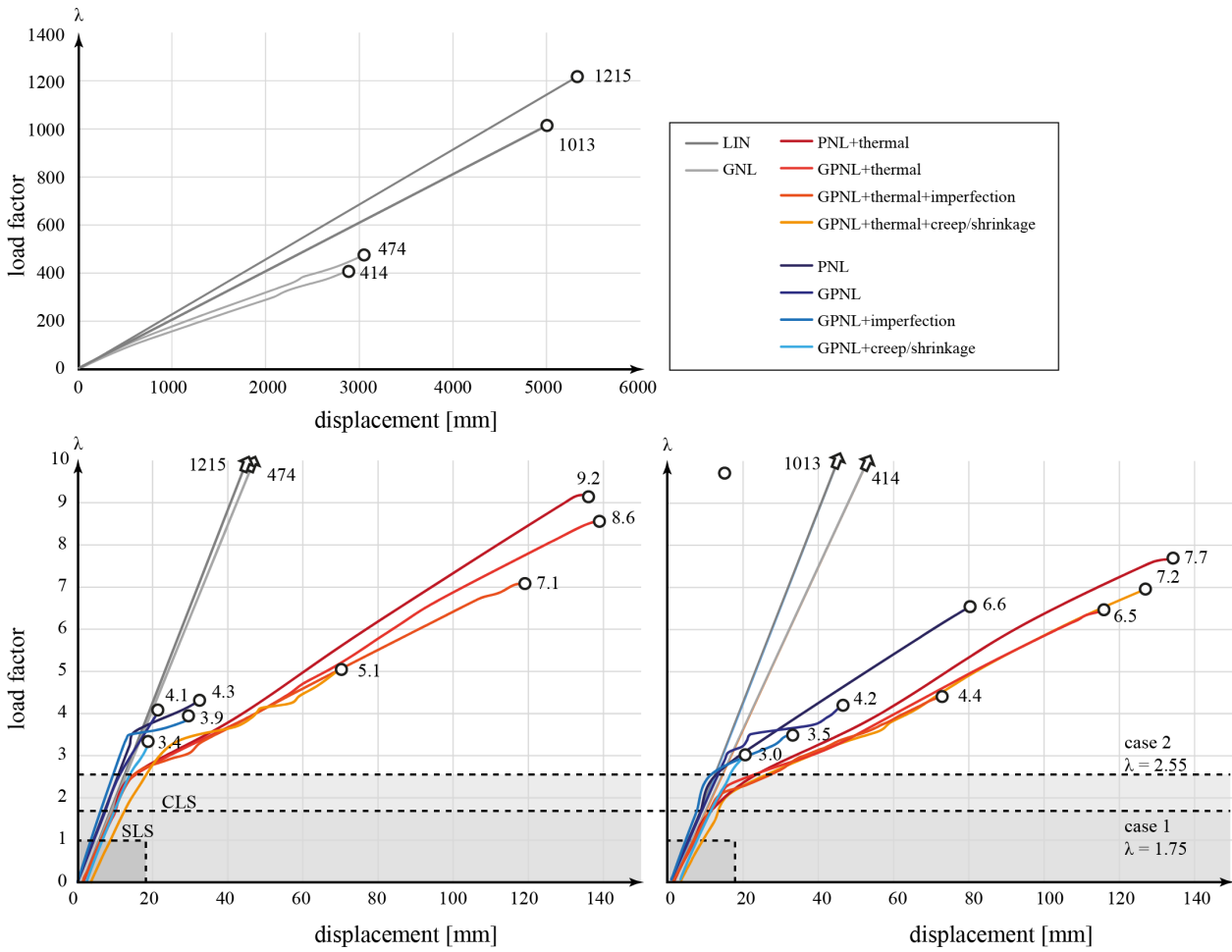


Figure 14: Load-deflection diagram for corner point for LC 1 and LC 4 without thermal loads, showing influence of various nonlinearities. LIN = linear, NL = nonlinear, P = physically, G = geometrically

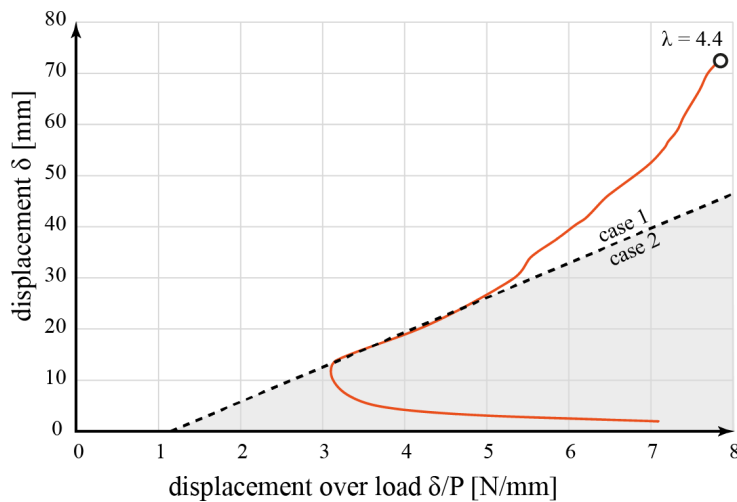


Figure 15: Southwell plot for LC 4 with imperfection, and thermal actions included, revealing increased post-buckling capacity

Figure 16 shows the front elevation and lower floor plan of the final design, which satisfies the, sometimes conflicting, objectives (Figure 13), and

was submitted to authorities for building permission.

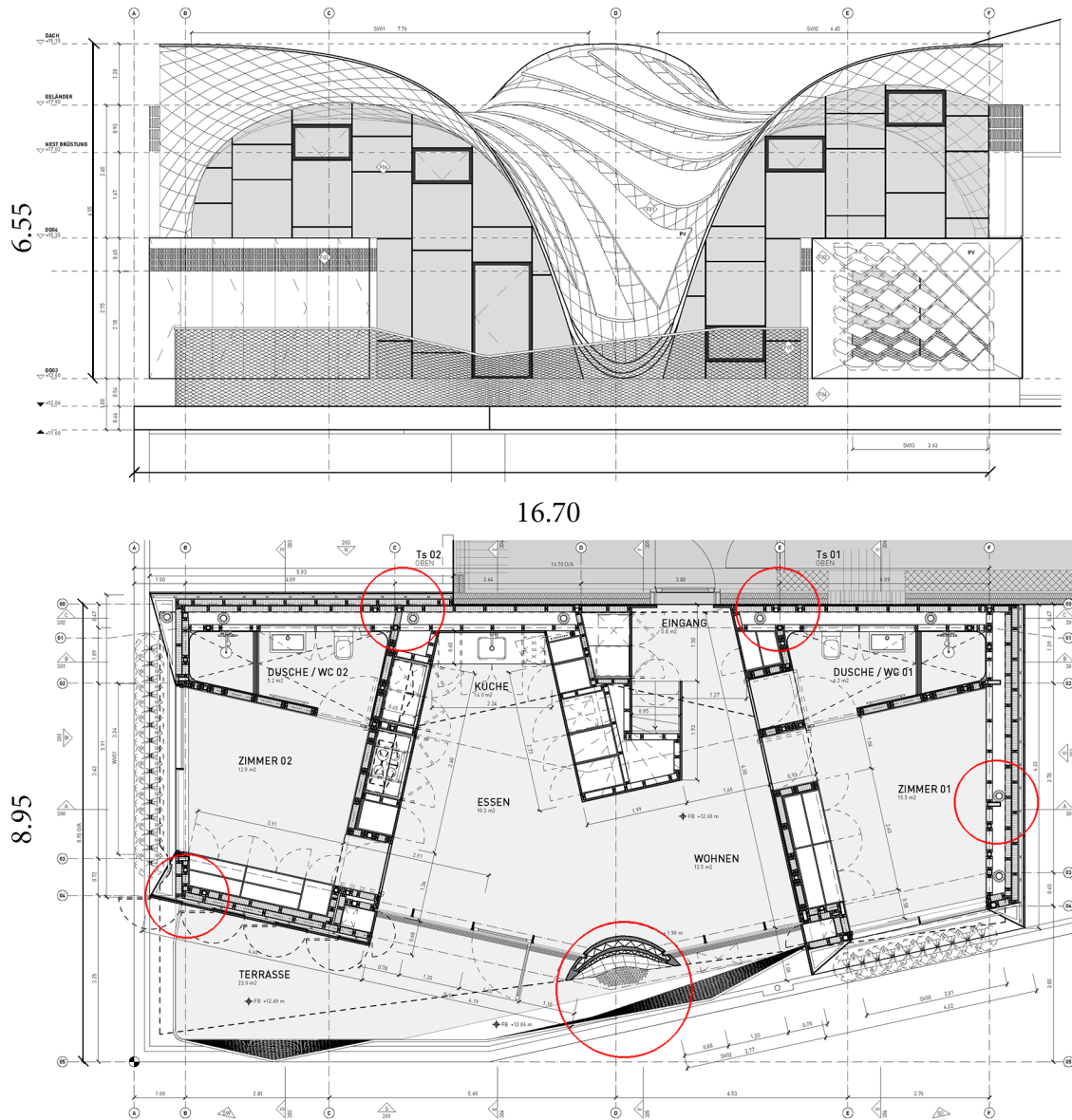


Figure 16: Front elevation and lower floor plan with main dimensions and location of supports in final design (drawings by Supermanoeuvre)

7. CONCLUSIONS

The structural design and geometry for the final design of a flexibly formed, mesh-reinforced sandwich shell roof, as part of the NEST HiLo project, has been presented, and will be handed over to Bollinger + Grohmann Ingenieure for detailed engineering in the next phase. Construction details will be dependent on further development within the design team and outcome of the tendering phase. The final design shown here is the specific result of a sequence of single- and later multi-criteria evolutionary optimization, evaluating various parameters related to structural and energy

performance, as well as architectural, spatial and constructional constraints. Further engineering was carried out to incorporate additional nonlinearities necessary to assess the strength, stiffness and stability of the shell according to Swiss codes, American codes for ferrocement, and IASS recommendations for concrete shells. Meanwhile, the optimization process and NEST HiLo's unique geometry demonstrate the potential of greater design freedom for anticlastic shell structures when using a flexible formwork. The final construction of NEST HiLo, planned for 2016, will allow the evaluation of other objectives, particularly cost efficiency and energy performance.

ACKNOWLEDGMENTS

The authors would like to acknowledge other members of the core design team who were influential in terms of the roof development and its constraints: Dave Pigram and Iain Maxwell from Supermanoeuvre; Rob Torsing and Jochem Verbeek from ZJA; as well as Prof. Arno Schlüter, Gearóid Lydon and Johannes Hofer from A/S.

Tim Chen corresponded with us on shell buckling while finishing his Master thesis [2], allowing us to benchmark Sofistik against his results. Finally, Prof. Agnes Weilandt shared information on her engineering approach of the Rolex Learning Centre [8], specifically how Sofistik was used to model creep and shrinkage.

REFERENCES (CODES)

- ACI 549R-97 [Reapproved 2009], Report on Ferrocement, American Concrete Institute, 1997.
- ACI 549.1R-93 [Reapproved 2009], Guide for the Design, Construction, and Repair of Ferrocement, American Concrete Institute, 1993.
- EN 1992-1-1:2004 Eurocode 2: Design of concrete structures - Part 1-1: General rules and rules for buildings. European Committee for Standardisation, 2004.
- IAASS 1979. See Medwadowski, 1979.
- SIA 260:2003 Basis of Structural Design. Swiss Standards Association, 2004.
- SIA 261:2003 Actions on Structures. Swiss Standards Association, 2003.
- SIA 262:2003 Concrete Structures. Swiss Standards Association, 2004.

REFERENCES

- [1] **Andersen, M.S., Dahl, J. and Vandenberghe, L.**, CVXOPT, <http://cvxopt.org>, 2014.
- [2] **Chen, T.**, On Introducing Imperfection in the Non-Linear Analysis of Buckling of Thin Shell Structures, Master thesis, TU Delft, Netherlands, 2014.

- [3] **Eisenbach, P., Vasudevan, R., Grohmann, M., Bollinger, K. and Hauser, S.**, 2014. Parapluie - Realisierung einer ultraschlanken Betonschale durch Aktivierung einer Membrantragwirkung. *Beton- und Stahlbau*, 109 [1], pp. 53-59.
- [4] **Flint A.R. and Low A.E.**, The construction of hyperbolic paraboloid type shells without temporary formwork. *Bulletin of the International Association for Shell Structures*, 1960; (4); 5-18.
- [5] **Flint, A.R.**, 1961. Some model tests on shell structures as an aid to design. *Proceedings of the Symposium on Shell Research*, August 30 – September 2, pp. 291-301.
- [6] **Gallegos-Cazeres, S. and Schnobrich, W.C.**, 1988. Effects of Creep and Shrinkage on the Behavior of Reinforced Concrete Gable Roof Hyperbolic-Paraboloids. University of Illinois. Structural Research Series No. 543.
- [7] **Garrido, M., Correia, J.R., Branco, F.A. and Keller, T.** Creep behaviour of sandwich panels with rigid polyurethane foam core and glass-fibre reinforced polymer faces: Experimental tests and analytical modelling. *Journal of Composite Materials* 2014; 48 (18): 2237-49. [DOI: 10.1177/0021998313496593]
- [8] **Grohmann, M., Bollinger, K., Weilandt, A. and Wagner, M.**, Form finding of the shell structures of the ROLEX Learning Center in Lausanne, *Proceedings of the International Association for Shells and Spatial Structures (IAASS) Symposium 2009*, Valencia, Spain.
- [9] **Hoogenboom, P.** Stability of Shells. CT4143 lecture handout, TU Delft.
- [10] **Jadik, T. and Billington, D.P.**, 1995. Gabled hyperbolic paraboloid roofs without edge beams. *Journal of Structural Engineering*, 121 [2], pp. 328–35. [DOI: 10.1061/(ASCE)0733-9445(1995)121:2(328)]
- [11] **Kollár, L.**, 1969. On the behaviour of shells in the postbuckling range. *In Bulletin of the International Association for Shell Structures*, [39], pp. 41-51.
- [12] **Kollár, L. and Dulácska, E.**, 1984. *Buckling of Shells for Engineers*. John Wiley & Sons.

- [13] **Maddex, D.**, 2007. Dow Alden B. Midwestern modern. Archetype Press.
- [14] **McNeel, R.**, Rhinoceros, <http://www.rhino3d.com>, Robert McNeel & Associates, 2014.
- [15] **Medwadowski S.J.**, Buckling of concrete shells: an overview. *Journal of the International Association for Shell and Spatial Structures*, 2004; 45(1): 51–63.
- [16] **Medwadowski, S.J. et al.** Recommendations for Reinforced Concrete Shells and Folded Plates. International Association for Shells and Spatial Structures, 1979.
- [17] **Meyer C. and Sheer M.H.**, Do concrete shells deserve another look? Industry professionals give mixed opinions. *Concrete International*, 2005; October; 43-50.
- [18] **Naaman, A.E.**, Ferrocement and Laminated Cementitious Composites. Techno Press, 2000.
- [19] NEST - Exploring the future of buildings. 2015. [ONLINE] Available at: <http://nest.empa.ch/en/>. [Accessed 26 May 15].
- [20] **Ortega, N.F. and Robles, S.I.**, 2003. The design of hyperbolic paraboloids on the basis of their mechanical behaviour. *Thin-Walled Structures*, 41, pp. 769–84. [DOI: 10.1016/S0263-8231(03)00025-9]
- [21] **Pauletti R.M.O. and Pimenta P.M.**, The natural force density method for the shape finding of taut structures, *Computer Methods in Applied Mechanics and Engineering*, 2008; 197; 4419-4428. [DOI: 10.1016/j.cma.2008.05.017]
- [22] **Rutten, D.**, Grasshopper, <http://www.grasshopper3d.com>, 2015.
- [23] **Schek H.-J.**, The force density method for form finding and computation of general networks. *Computer Methods in Applied Mechanics and Engineering*, 1974; 3; 115-134. [DOI: 10.1016/0045-7825(74)90045-0]
- [24] **Schneider, H.N.**, Entwicklung von Demonstrator-Bauteilen aus textilbewehrtem Beton. Allgemeine Angaben zum beendeten Teilprojekt E4. pp. 391-415, 2011.
- [25] **Tomás, A. and Martí, P.** Optimality of candela's concrete shells, a study of his posthumous design. *Journal of the International Association of Shells and Spatial Structures* 2010; 51(1): 67–77.
- [26] **Tomás, A. and Tovar J.P.**, The influence of initial geometric imperfections on the buckling load of single and double curvature concrete shells. *Computers and Structures*, 2012; 96-97; 34–45. [DOI: 10.1016/j.compstruc.2012.01.007]
- [27] **Van Mele T. and Block P.**, Novel form finding method for fabric formwork for concrete shells. *Journal of the International Association of Shells and Spatial Structures* 2011; 52(4):217–24.
- [28] **Van Mele, T., Panozzo, D., Sorkine-Hornung, O. and Block, P.**, 2014. Best-fit thrust network analysis. Rationalization of freeform meshes. In *Shell Structures for Architecture. Form Finding and Optimization*. eds. Adriaenssens, S., Block, P., Veenendaal, D. and Williams, C. Routledge.
- [29] **Veenendaal D. and Block P.**, Design process for prototype concrete shells using a hybrid cable-net and fabric formwork. *Engineering Structures* 2014; 75:39-50. [DOI: 10.1016/j.engstruct.2014.05.036]
- [30] **Veenendaal D., Bezbradica M., Novak D. and Block P.**, Controlling the geometry and forces of hybrid cable-net and fabric formworks. *Proceedings of the IASS-SLTE 2014 Symposium*, Brasilia; 2014.
- [31] **Waling, J. and Greszczuk, L.**, 1960. Experiments with thinshell structural models. *Proceedings, annual meeting, American Concrete Institute*, 57, pp. 413–31.
- [32] **Waling J., Ziegler E. and Kemmer H.**, Hy-par shell construction by offset wire method. *Proceedings, World Conference on Shell Structures*. San Francisco, CA, US; 1962; October 1-4; 453-462.